

Constrained Attitude Maneuvers on $SO(3)$: Rotation Space Sampling, Planning and Low-Level Control [★]

Xiao Tan ^a, Soulaymane Berkane ^b, Dimos V. Dimarogonas ^a

^a*Division of Decision and Control Systems, School of Electrical Engineering and Computer Science, KTH Royal Institute of Technology, SE-100 44, Stockholm, Sweden*

^b*Département d'informatique et d'ingénierie, Université du Québec en Outaouais, J8X 3X7, Québec, Canada*

Abstract

In this paper, we propose a novel framework that provides a systematic strategy to regulate the rigid body attitude on $SO(3)$ within a generic constrained attitude zone. The proposed control scheme consists of three components: sampling, planning and low-level control. Specifically, an overlapping cell-like sampling for the attitude configuration space $SO(3)$ is built and further reformulated to a graph model. Based on this abstraction, a complete graph search algorithm is utilized to generate a feasible path in the graph model. Both sufficient and necessary conditions on finding a feasible path are presented. Furthermore, to facilitate the control design, the point-to-point path is transformed into a smooth reference trajectory along the geodesics. Finally, a saturated low-level control law is formulated to robustly track the desired trajectory. Simulations demonstrate the effectiveness of the proposed control approach.

Key words: Constrained attitude maneuvers; Special orthogonal group; Sampling and abstraction on $SO(3)$; Trajectory planning; Resolution completeness; Saturation control;

1 Introduction

The attitude (orientation) control problem dates back to the early space and aerial applications which are mainly related to spacecraft and aircraft attitude regulation. With the recent advances in applications of unmanned aerial and underwater vehicles (*e.g.*, UAVs, AUVs), the effective attitude control of these vehicles becomes crucial for their successful operation. Recent works in the area of attitude control have focused on the use of Lie group methods on the special orthogonal group $SO(3)$ (the attitude configuration space) to study this control problem from a differential geometric perspective [1–4]. This is motivated by the fact that all existing parameterizations fail to represent the attitude of a rigid body both globally and uniquely, which results in control schemes that are either singular or exhibit some undesirable be-

havior (*e.g.*, unwinding phenomenon).

The study of the attitude control problem in the presence of constraints (*i.e.*, unfeasible rotational regions) has received less attention in the literature. This problem is a specific case of a state-constrained nonlinear control problem and consists of designing a controller to regulate the attitude of the rigid body to the desired orientation, while actively avoiding certain orientation configurations. The constrained attitude control problem is motivated, *e.g.*, in aerospace applications where a space telescope observes some celestial regions while avoiding bright stars [5]. Another example of application is encountered when an unmanned vehicle or robot manipulator is navigating in cluttered environments which constrains both its attitude and position.

Different control schemes have been proposed in the last decade for the constrained attitude maneuver problem. Generally speaking, they can be categorized into two types: potential function based methods [6–8] and path planning based methods [9,10]. The potential function based method defines a judiciously selected potential function that associates a scalar with every attitude. When the attitude state approaches the constrained zone, the potential value gets larger; and when approaching the desired attitude, the potential value de-

[★] This work was supported by the H2020 ERC Starting Grant BUCOPHSYS, the EU H2020 Research and Innovation Programme under GA No. 731869 (Co4Robots), the SSF COIN project, the Swedish Research Council (VR) and the Knut och Alice Wallenberg Foundation.

Email addresses: xiaotan@kth.se (Xiao Tan), soulaimane.berkane@uqo.ca (Soulaymane Berkane), dimos@kth.se (Dimos V. Dimarogonas).

creases. The desired attitude is typically set to be the global minimum. The attitude control law is then formulated using the negative gradient of the potential function. This method generally provides a robust feedback controller that is easy for implementation. However, some notable disadvantages of the potential-based methods are 1) the attitude maneuvers may get trapped into local minima instead of approaching the global minimum (i.e., the desired attitude) [11], and 2) they generally deal with a conic or convex shape of the constrained zone [6].

The existing path planning based methods, on the other hand, are somehow computationally expensive for implementation. For example, the randomized planning algorithm [9] is time-consuming and not suitable for on-board implementations. Recently, deterministic planning schemes were proposed in [10], where the rotational space was discretized using the quaternion representation. The attitude space was sampled into discretized points and then those points were connected to form a semi-feasible path. However, it is not guaranteed that the path between two consecutive points will comply with the attitude constraints, while the nonlinear dynamics is also omitted. To the authors' best knowledge, there is no existing work that considers search-based planning in the rotation space $SO(3)$. The main difficulty is the intrinsic geometric properties of $SO(3)$, which forms a curved 3-dimensional manifold embedded in $\mathbb{R}^{3 \times 3}$. In fact, the definition of a uniform distribution sampling over $SO(3)$ varies in the literature [12–14]. In [15], the authors predefine an analytical form of the attitude trajectory and use a trial-and-error procedure to iteratively update the parameters against a safety criterion, which is applicable only for small obstacle regions. Moreover, in all aforementioned schemes, feasibility guarantees are missing.

In this paper, we develop a framework for the constrained attitude maneuver problem on the rotation space $SO(3)$. The proposed framework consists of three stages: configuration space sampling, trajectory planning and low-level control; all are carried out directly on the Lie group $SO(3)$ thus avoiding issues related to ambiguities and singularities of other attitude parametrizations. This attitude maneuver is achieved such that, during the maneuver, the attitude avoids certain rotational areas (constrained zones) while the control torques satisfy an *a priori* bound. Note that in contrast to potential function-based methods, which usually deal with particular types of constraints, here we consider generic attitude constrained zones.

The contributions of this paper are described hereafter. First, we construct overlapping *sampling cells* that cover the whole manifold $SO(3)$ with some benign properties that are crucial for the construction of a valid graph abstraction. Each constructed cell is centered around a sampling point on $SO(3)$ generated using the approach of [12]. Another interesting feature of the proposed cell

partitioning is that, for any two neighbouring sampling rotations, or any two rotations within the same cell, the *geodesic attitude maneuvering* between them stays within the given cell(s). This property allows to obtain a continuous path over the configuration manifold $SO(3)$ from a given path over the abstracted graph. Then, based on the proposed cell abstraction, we model the unconstrained zone as an undirected graph and search algorithms are used to generate a feasible path over the graph. Next, we give necessary and sufficient conditions for the existence of a feasible path in $SO(3)$ that solves the constrained attitude maneuver problem. Finally, a smooth reference trajectory is constructed from the obtained feasible path and a saturated low-level control law is used to robustly track the reference trajectory.

2 Notations and Preliminaries

The sets of real, non-negative real and positive integer numbers are denoted as $\mathbb{R}, \mathbb{R}_{\geq}, \mathbb{N}$, respectively. \mathbb{R}^n denotes the n -dimensional Euclidean space. For any vectors $x, y \in \mathbb{R}^n$, their inner product is defined as $\langle x, y \rangle := x^\top y$. The 2-norm of a vector x is $\|x\|_2 := \sqrt{x^\top x}$. The Frobenius norm of A is defined as $\|A\|_F := \sqrt{\text{tr}(A^\top A)}$, where $\text{tr}(\cdot)$ denotes the trace of a matrix. I is the 3-dimensional identity matrix. Let \mathbb{S}^n denote the n -dimensional unit sphere $\mathbb{S}^n := \{x \in \mathbb{R}^{n+1} \mid \|x\|_2 = 1\}$.

Any rotation matrix is an element of the Special Orthogonal group $SO(3) := \{R \in \mathbb{R}^{3 \times 3} \mid R^\top R = RR^\top = I, \det(R) = 1\}$ which, when associated with the matrix multiplication operation, forms a Lie group. The associated Lie algebra, denoted as $\mathfrak{so}(3)$, consists of the set of all skew-symmetric 3×3 matrices, i.e., $\mathfrak{so}(3) := \{\Omega \in \mathbb{R}^{3 \times 3} \mid \Omega^\top = -\Omega\}$. The map $[(\cdot)]_\times : \mathbb{R}^3 \rightarrow \mathfrak{so}(3)$ and its inverse map $\vee : \mathfrak{so}(3) \rightarrow \mathbb{R}^3$ are explicitly defined as
$$x = \begin{bmatrix} x_1 \\ x_2 \\ x_3 \end{bmatrix} \xrightarrow{[(\cdot)]_\times} [x]_\times = \begin{bmatrix} 0 & -x_3 & x_2 \\ x_3 & 0 & -x_1 \\ -x_2 & x_1 & 0 \end{bmatrix}.$$

The Lie algebra $\mathfrak{so}(3)$ allows to represent rotation matrices on $SO(3)$ via the matrix exponential $\exp(\cdot)$.

For $[x]_\times \in \mathfrak{so}(3)$, $\exp([x]_\times) = I + \frac{\sin(\|x\|_2)}{\|x\|_2} [x]_\times + \frac{1 - \cos(\|x\|_2)}{\|x\|_2^2} [x]_\times^2$ when $x \neq 0$, and $\exp([x]_\times) = I$ otherwise [16]. For all rotation matrices R with $\text{tr}(R) \neq -1$, the exponential map admits an inverse logarithmic map given by $\log(R) = \frac{\theta(R)}{2 \sin(\theta(R))} (R - R^\top)$ when $R \neq I$,

and $\log(R) = 0$ otherwise, where $\theta(R)$ is the rotation angle associated to R and $\theta(R) := \arccos((\text{tr}(R) - 1)/2)$ [16]. Given two rotation matrices R_1 and R_2 with $\text{tr}(R_1 R_2^\top) \neq -1$, the *geodesic interpolation* between R_1 and R_2 is $R(\tau) := R_1 \exp(\tau \log(R_1^\top R_2))$, $0 \leq \tau \leq 1$, which defines a path connecting R_1 and R_2 . More generally, a *path* $F(\cdot)$ in \mathcal{A} connecting R_1 and R_2 , where \mathcal{A} is a subset of $SO(3)$, is defined as a continuous function

$F : [0, 1] \rightarrow \mathcal{A}$ with $F(0) = R_1$ and $F(1) = R_2$. If there exists such a path $F(\cdot)$, we say (R_1, R_2) is *connected*. For any $R_1, R_2 \in SO(3)$ with $\text{tr}(R_1 R_2^\top) \neq -1$, the *angular distance* is given by $d(R_1, R_2) := \|\log(R_1 R_2^\top)\|_2$.

3 Problem Formulation

3.1 Attitude Dynamics

The attitude dynamics of a rigid body are given by

$$\begin{cases} \dot{R} = R[\omega]_\times, \\ J\dot{\omega} + [\omega]_\times J\omega = u, \end{cases} \quad (1)$$

where $R \in SO(3)$ represents the attitude transformation from the body-fixed frame O_b to the inertia reference frame O , $\omega \in \mathbb{R}^3$ is the corresponding angular velocity expressed in the body-fixed frame O_b , J is the constant and known inertia matrix and $u \in \mathbb{R}^3$ is the input torque expressed in the body-fixed frame O_b . For practical implementations, the control torque u should satisfy the bound $\|u\|_2 \leq u_{\max}$, where u_{\max} is an *a priori* upper bound of the allowable control torque.

3.2 Constrained Attitude Control Problem

In many applications, attitude maneuvers of a rigid body need to be performed within a certain region of $SO(3)$. One motivating example from [5] is shown in Fig.1. The maneuver task is to point to stars, while the on-board sensor should avoid direct exposure to bright objects (the sun and the moon), and the spacecraft should maintain communication with the ground station.

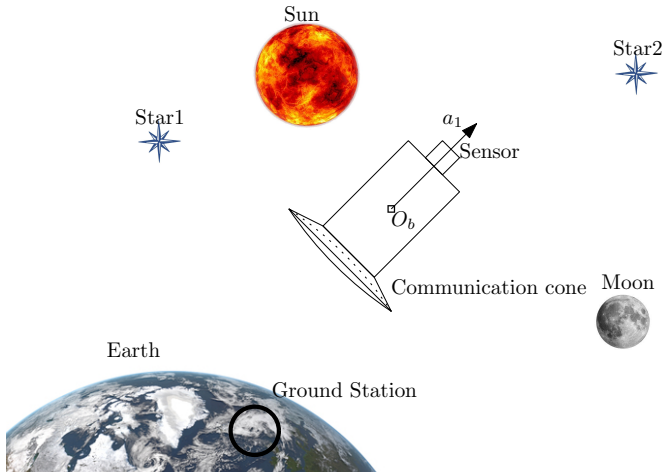


Fig. 1. A spacecraft to be maneuvered such that the sensor points from Star 1 to Star 2, while avoiding the sun and the moon, and maintaining communication with the ground station.

In this paper, we consider a generic keep-out region in $SO(3)$ denoted by $\mathcal{O} \subset SO(3)$. The corresponding active region is the complement of the constrained region and denoted by $\mathcal{A} = SO(3) \setminus \mathcal{O}$. Given the obstacle region

\mathcal{O} , the initial and the target attitude R_0 and R_f , the goal is to find a continuous control law u satisfying the allowable limit u_{\max} such that once the attitude starts at R_0 , the attitude will evolve within \mathcal{A} for all times and rest on R_f at time $0 \leq T_f < \infty$, i.e., the attitude trajectory should satisfy

$$\begin{cases} R(0) = R_0, \\ R(t) \in \mathcal{A} \text{ for } t \geq 0, \\ R(t) = R_f \text{ for } t \geq T_f. \end{cases} \quad (2)$$

Moreover, in certain scenarios, the attitude task above can be infeasible due to the obstacle region \mathcal{O} and in this case, our goal is to detect these situations and return infeasible.

To summarize, in this paper, we present a framework for the constrained attitude maneuver problem in (2). The control scheme consists of three components: 1) sampling cell construction; 2) cell-to-cell planning; 3) low-level control. In the following sections, we will give further details on each of these three modules.

4 Sampling Cells in $SO(3)$

In this section, we provide the details on constructing the sampling cells in $SO(3)$ with certain favorable properties. Let the sampling set $U := \{R_1, R_2, \dots, R_i, \dots, R_n\}$ be a finite set with n elements in $SO(3)$ and let $\mathcal{N} := \{1, 2, \dots, n\} \subset \mathbb{N}$ be an index set. For each $i \in \mathcal{N}$, define the cell region S_i as the open ball centered at R_i with a radius $\theta \in (0, \pi/2)$, i.e., $S_i := \{R \in SO(3) \mid d(R, R_i) < \theta\}$, $\forall i \in \mathcal{N}$. The neighborhood set N_i of a sampling point R_i is defined as $N_i := \{R \in U \mid d(R, R_i) < 2\theta, R \neq R_i\}$, $\forall i \in \mathcal{N}$, which contains all the sampling points other than R_i that lie within angular distance 2θ of R_i .

4.1 Sampling Set in $SO(3)$

An approach on generating sampling points in $SO(3)$ has been proposed by Mitchell[12]. We recall in the following the main ingredients of the method. In accordance with [12], we denote by \mathbb{S} either the space $\mathbb{S}^1, \mathbb{S}^2$ or $SO(3)$. The metric $d_E(v, w) := \|v - w\|_2$ for $v, w \in \mathbb{S}^1$ or $v, w \in \mathbb{S}^2$. For any $v, w \in SO(3)$, the *Euclidean distance* $d_E(v, w)$ is defined as $\|v - w\|_F / \sqrt{2}$.

Definition 1 ($\{s, \sigma\}$ -separated) A finite subset \mathcal{V} of \mathbb{S} is called $\{s, \sigma\}$ -separated if

$$\begin{aligned} \max_{w \in \mathcal{V}} \left(\min_{v \in \mathcal{V}, v \neq w} d_E(v, w) \right) &\leq \sigma s, \\ \min_{w \in \mathcal{V}} \left(\min_{v \in \mathcal{V}, v \neq w} d_E(v, w) \right) &\geq s / \sigma, \end{aligned} \quad (3)$$

where s is the sampling length step, and $\sigma \geq 1$.

Definition 1 states the local distribution properties of the sampling points. If $\sigma \approx 1$, the distribution of sampling points is considered as not too dense nor too coarse.

Definition 2 ($\{s, \rho\}$ -covered) *A finite subset \mathcal{V} of \mathbb{S} is called $\{s, \rho\}$ -covered if*

$$\sup_{w \in \mathbb{S}} \left(\min_{v \in \mathcal{V}} d_E(v, w) \right) \leq \rho \sqrt{\dim \mathbb{S}} s / 2, \quad (4)$$

where s is the sampling length step, $\rho > 0$, and $\dim(\mathbb{S})$ is the dimension of \mathbb{S} , where $\dim \mathbb{S}^1 = 1$, $\dim \mathbb{S}^2 = 2$ and $\dim SO(3) = 3$.

Definition 2 considers the covering property, since it defines the maximum distance between an arbitrary element in \mathbb{S} and a sampled point in \mathcal{V} . These two uniformity measures can be easily extended to other spaces. For example, for a regular lattice in \mathbb{R}^3 , the corresponding values are $\sigma = 1, \rho = 1$.

For any given sampling step s and a finite subset $U \subset SO(3)$, a lower bound on σ can be calculated from (3) to guarantee that the set U is $\{s, \sigma\}$ -separated. The value $\sup_{w \in SO(3)} \min_{v \in U} d_E(v, w)$ is obtained via numerical method (by choosing w arbitrarily from $SO(3)$ with a large number of trials), thus ρ can be calculated in view of (4).

Algorithm 1 Sampling set algorithm.

Input: sampling step s

Output: sampling set U

```

initialize:
1:  $U = \{ \}$ 
   construct the sampling set in  $SO(3)$ :
2: construct the sampling set  $V^1, V^2$  on  $\mathbb{S}^1, \mathbb{S}^2$ 
3: for  $v$  in  $V^2$  do
4:    $r_3 \leftarrow v$ 
5:   pick  $M \in SO(3)$  such that  $M(0, 0, 1)^\top = r_3$ 
6:   for  $w = (w_1, w_2)$  in  $V^1$  do
7:      $r_2 \leftarrow M(w, 0)^\top, r_1 \leftarrow r_2 \times r_3$ 
8:      $R = (r_1, r_2, r_3), U \leftarrow U \cup \{R\}$ 
9:   end for
10: end for
11: return  $U$ 

```

In [12], the author provides a method to generate the sampling set on $SO(3)$ based on the finite discrete sample sets $V^1 \subset \mathbb{S}^1$ and $V^2 \subset \mathbb{S}^2$, which are generated by minimizing a repulsive potential

$$E = \sum_{i=1}^{k-1} \sum_{j=i+1}^k d_E^{-1}(v_i, v_j) \text{ with } v_i, v_j \in V^1 \text{ or } v_i, v_j \in V^2,$$

where the cardinality k depends on the sampling step s . The sampling algorithm is summarized in Algorithm 1. Software for implementing Algorithm 1 and generating the sampling points in $SO(3)$ is accessible from the website¹. One sampling set example is given later.

4.2 Construction of the Sampling Cells

In this subsection, we use the sampling points on $SO(3)$ generated by Algorithm 1 to construct the intercon-

¹ <https://mitchell-lab.biochem.wisc.edu/SOI/index.php>

nected sampling cells S_i . These sampling cells cover the whole space $SO(3)$ with some other favorable properties as expressed in Theorem 1.

Theorem 1 *Suppose $U \subset SO(3)$ to be a finite sampling set, which is $\{s, \sigma\}$ -separated and $\{s, \rho\}$ -covered such that s, σ, ρ satisfy the following inequalities:*

$$\begin{cases} \arcsin(\sigma s / 2) < 2 \arcsin(s / (2\sigma)) \\ \rho \sigma < 2 / \sqrt{3} \end{cases} \quad (5)$$

Let θ be the radius of the open cells S_i . Choose θ such that $\max(\arcsin(\sigma s / 2), 2 \arcsin(\sqrt{3}\rho s / 4)) < \theta < 2 \arcsin(s / 2\sigma)$. Then the sampling set U has the following properties

- i. For all $i \in \mathcal{N}, N_i \neq \emptyset$;
- ii. For all $i, j \in \mathcal{N}, i \neq j$, we have $R_j \notin S_i$;
- iii. For all $R_i \in U$, and all $R_j \in N_i, \theta < d(R_i, R_j) < 2\theta$
- iv. $\bigcup_{i \in \mathcal{N}} S_i = SO(3)$.

Property (i) of Theorem 1 shows that every sampling cell S_i has some neighboring sampling cells, e.g. S_j . Property (ii) further states that the center point R_j is guaranteed to be outside of the cell S_i for any neighboring cells S_i and S_j . These two properties are concluded in property (iii), stating that every pair of neighboring sampling points R_i and R_j satisfies $\theta < d(R_i, R_j) < 2\theta$. Finally, property (iv) shows that the union of all the obtained sampling cells covers the whole space $SO(3)$.

PROOF. Note that for any two elements $v, w \in SO(3)$ with $\text{tr}(vw^\top) \neq -1$, $d_E(v, w) = 2 \sin(d(v, w)/2)$ holds [12]. Thus $d_E(v, w)$ can be seen as a function with respect to $d(v, w)$, which, as $d(v, w) \in [0, \pi)$, is a monotonically increasing function. Since U is $\{s, \sigma\}$ -

separated, by definition, $\max_{w \in U} \left(\min_{v \in U, v \neq w} d_E(v, w) \right) \leq \sigma s$

and $\min_{w \in U} \left(\min_{v \in U, v \neq w} d_E(v, w) \right) \geq s / \sigma$.

Invoking the relation between the Euclidean distance and the angular distance, we have

$$\max_{w \in U} \left(\min_{v \in U, v \neq w} d(v, w) \right) \leq 2 \arcsin(\sigma s / 2), \quad (6)$$

$$\min_{w \in U} \left(\min_{v \in U, v \neq w} d(v, w) \right) \geq 2 \arcsin(s / (2\sigma)). \quad (7)$$

As U is $\{s, \rho\}$ -covered, invoking the relation between the two distance metrics again, we have

$$\sup_{w \in SO(3)} \left(\min_{v \in U} d(v, w) \right) \leq 2 \arcsin(\sqrt{3}\rho s / 4). \quad (8)$$

Choose θ such that $\max\left(\arcsin(\sigma s/2), 2\arcsin(\sqrt{3}\rho s/4)\right) < \theta < 2\arcsin(s/2\sigma)$, which is feasible due to (5) with some straightforward calculation. Then the properties in Theorem 1 can be shown by contradiction.

- 1) Suppose that there exists $j \in \mathcal{N}$ such that $N_j = \emptyset$. This implies that for all $i \in \mathcal{N}, i \neq j$, $d(R_i, R_j) \geq 2\theta > 2\arcsin(\sigma s/2)$. However, since U is assumed to be $\{s, \sigma\}$ -separated, this contradicts with (6). Thus no such j exists, which completes the proof of property (i).
- 2) Suppose that there exist $i, j \in \mathcal{N}, i \neq j$, and $R_j \in S_i$, then $d(R_i, R_j) < \theta < 2\arcsin(s/(2\sigma))$. However, since U is assumed to be $\{s, \sigma\}$ -separated, this contradicts with (7). Thus property (ii) is proven.
- 3) Property (iii) is a straightforward conclusion from (i) and (ii).
- 4) Suppose that there exists an attitude $R' \in SO(3)$ such that $R' \notin \bigcup_{i \in \mathcal{N}} S_i$. It implies that $d(R_i, R') \geq \theta$ for all $i \in \mathcal{N}$, and then $d(R_i, R') > 2\arcsin(\sqrt{3}\rho s/4), \forall i \in \mathcal{N}$, which contradicts with (8). Thus property (iv) holds. \square

Remark 1 Suppose, for some s , the distribution parameters σ and ρ of the sampling provided by Algorithm 1 cannot satisfy (5). Then s should be tuned. Although we do not provide a theoretical guarantee that for all s , the generated samplings will satisfy (5), a numerical result for arbitrary s is shown in Fig. 2, where the shaded area denotes the region of feasible (ρ, σ) pairs.

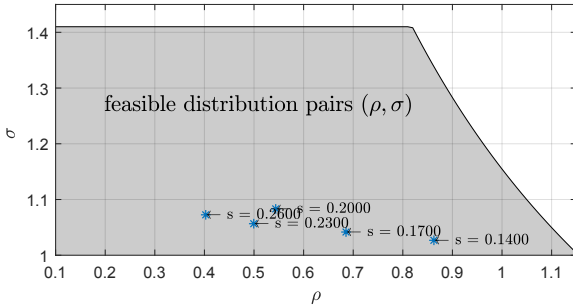


Fig. 2. Numerical result of feasible (ρ, σ) pairs.

Example 1 Choosing $s = 0.2567$, the distribution parameters of the sampling set U are $\sigma = 1.017, \rho = 0.95$ with $n = 4392$. Thus, one possible θ is 13 degrees.

In the following, we assume that a sampling set satisfying (5) has been found and the properties (i)~(iv) in Theorem 1 will be used as a base stone.

4.3 Attitude Sub-Maneuvers Design

Before presenting the planning algorithm on the cell level, we introduce two types of attitude maneuvers: 1) the attitude traverses from one cell to a neighboring cell and 2) the attitude maneuvers within one cell. We next show in the following propositions that, for any two

neighbouring sampling rotations, or any two rotations within the same cell, the geodesic path between them stays within the given cell(s). This is an important property for the validity of the graph abstraction that will be discussed in the next section.

Proposition 1 The interpolation along geodesics on $SO(3)$ between two neighboring sampling rotations R_i and R_j is within $S_i \cup S_j$.

PROOF. From Theorem 1, for any sampling point R_i , and any sampling point $R_j \in N_i$, we have $\theta < d(R_i, R_j) < 2\theta$, with $\theta < \pi/2$. Let $d(R_i, R_j) := \theta_1$. The geodesic path from R_i to R_j is $R_{i,j}(\tau) = R_i \exp(\tau \log(R_i^\top R_j))$ for $0 \leq \tau \leq 1$. Thus $\log(R_i^\top R_{i,j}(\tau)) = \tau \log(R_i^\top R_j)$. For $0 \leq \tau \leq 1/2$, $d(R_i, R_{i,j}(\tau)) = \|\log(R_i^\top R_{i,j}(\tau))\|_2 = \tau \|\log(R_i^\top R_j)\|_2 = \tau \theta_1 \leq \theta_1/2 < \theta$. Thus $R_{i,j}(\tau) \in S_i$ for $\tau \in [0, 1/2]$ by definition. Similarly, it can be verified that for $\tau \in [1/2, 1]$, $R_{i,j}(\tau) \in S_j$. Thus up to $\tau = 1/2$, the interpolation is in S_i , and enters and stays in S_j for $\tau \geq 1/2$. \square

Proposition 2 For any cell $S_i, i \in \mathcal{N}$ and two arbitrary points $R_{i1}, R_{i2} \in S_i$, the geodesic path between R_{i1} and R_{i2} is within S_i .

PROOF. In the proof we need to use unit quaternion representation. A unit quaternion is defined by the vector $\mathbf{Q} := (\eta, \mathbf{q}) \in \mathbb{S}^3$ such that $\eta \in \mathbb{R}$ is the scalar part and $\mathbf{q} \in \mathbb{R}^3$ is its vector part. Let $\mathbf{Q}_1 = (\eta_1, \mathbf{q}_1)$ and $\mathbf{Q}_2 = (\eta_2, \mathbf{q}_2)$ be two unit quaternions corresponding to the rotation matrices R_1 and R_2 , respectively. The quaternion multiplication is defined by $\mathbf{Q}_1 \cdot \mathbf{Q}_2 := (\eta_1 \eta_2 - \langle \mathbf{q}_1, \mathbf{q}_2 \rangle, \eta_1 \mathbf{q}_2 + \eta_2 \mathbf{q}_1 + \mathbf{q}_1 \times \mathbf{q}_2)$. By letting $\mathbf{Q}_I = (1, 0, 0, 0)$ to be the unit identity quaternion, the inverse of a unit quaternion \mathbf{Q} is defined as $\mathbf{Q}^{-1} = (\eta, -\mathbf{q})$. With a slightly abuse of notation, we define the angular distance between the two quaternions as $d(\mathbf{Q}_1, \mathbf{Q}_2) := 2 \arccos(|\eta_1 \eta_2 + \langle \mathbf{q}_1, \mathbf{q}_2 \rangle|)$. It can be verified that $d(\mathbf{Q}_1, \mathbf{Q}_2) = d(\mathbf{Q}_I, \mathbf{Q}_I^{-1} \mathbf{Q}_2) = d(R_1, R_2)$ [17]. For more about unit quaternion and the representation conversion, readers may refer to [17] for details.

$R_{i1}, R_{i2} \in S_i$ implies that $d(R_{i1}, R_i) < \theta$ and $d(R_{i2}, R_i) < \theta$. From the triangle inequality of the angular distance, it holds that $d(R_{i1}, R_{i2}) < 2\theta < \pi$. Choose $\mathbf{Q}_i, \mathbf{Q}_{i1}, \mathbf{Q}_{i2}$ to be the corresponding quaternions of R_i, R_{i1}, R_{i2} , where $\langle \mathbf{Q}_i, \mathbf{Q}_{i1} \rangle \geq 0, \langle \mathbf{Q}_i, \mathbf{Q}_{i2} \rangle \geq 0, \langle \mathbf{Q}_{i1}, \mathbf{Q}_{i2} \rangle \geq 0$ as vectors in \mathbb{R}^4 . If $\mathbf{Q}_{i1} = \mathbf{Q}_{i2}$, the interpolation is trivial. Otherwise, the interpolation from \mathbf{Q}_1 to \mathbf{Q}_2 along geodesics is given by [18] $\mathbf{Q}(\tau) = (\sin((1-\tau)\gamma)\mathbf{Q}_{i1} + \sin(\tau\gamma)\mathbf{Q}_{i2})/\sin(\gamma), 0 \leq \tau \leq 1$, where $\gamma = \arccos(\langle \mathbf{Q}_{i1}, \mathbf{Q}_{i2} \rangle) \in (0, \pi/2)$. Thus, $\mathbf{Q}_i^{-1} \cdot \mathbf{Q}(\tau) = \mathbf{Q}_i^{-1} \cdot (\sin((1-\tau)\gamma)\mathbf{Q}_{i1} + \sin(\tau\gamma)\mathbf{Q}_{i2})/\sin(\gamma)$. Note that for any quaternions $\mathbf{Q}_1, \mathbf{Q}_2, \mathbf{Q}_3$, the product distribution law holds, i.e., $\mathbf{Q}_1 \cdot (\mathbf{Q}_2 + \mathbf{Q}_3) =$

$\mathbf{Q}_1 \cdot \mathbf{Q}_2 + \mathbf{Q}_1 \cdot \mathbf{Q}_3$. Thus, $\mathbf{Q}_i^{-1} \cdot \mathbf{Q}(\tau) = (\sin((1 - \tau)\gamma)\mathbf{Q}_i^{-1} \cdot \mathbf{Q}_{i1} + \sin(\tau\gamma)\mathbf{Q}_i^{-1} \cdot \mathbf{Q}_{i2})/\sin(\gamma)$.

Without loss of generality, assume $d(R_{i1}, R_i) \leq d(R_{i2}, R_i) := \alpha < \theta$. Considering only the scalar components $\eta_{\tau,0}, \eta_{1,0}, \eta_{2,0}$ of $\mathbf{Q}_i^{-1} \cdot \mathbf{Q}(\tau), \mathbf{Q}_i^{-1} \cdot \mathbf{Q}_{i1}, \mathbf{Q}_i^{-1} \cdot \mathbf{Q}_{i2}$, we have $\eta_{1,0} \geq \eta_{2,0} = \cos(\alpha/2)$ and thus $\eta_{\tau,0} = (\sin((1 - \tau)\gamma)\eta_{1,0} + \sin(\tau\gamma)\eta_{2,0})/\sin(\gamma) \geq \cos(\alpha/2)(\sin((1 - \tau)\gamma) + \sin(\tau\gamma))/\sin(\gamma)$, $0 \leq \tau \leq 1$. With some calculations, it can be shown that for $0 \leq \tau \leq 1, 0 < \gamma < \pi/2$, $(\sin((1 - \tau)\gamma) + \sin(\tau\gamma))/\sin(\gamma) \geq 1$ holds. Thus $\eta_{\tau,0} \geq \cos(\alpha/2)$ for $0 \leq \tau \leq 1$. This leads to $d(\mathbf{Q}(\tau), \mathbf{Q}_i) \leq \max(d(\mathbf{Q}_{i1}, \mathbf{Q}_i), d(\mathbf{Q}_{i2}, \mathbf{Q}_i)) = \alpha < \theta, 0 \leq \tau \leq 1$, i.e., the interpolation along geodesics between R_{i1} and R_{i2} is within S_i . \square

Propositions 1 and 2 indicate that once we have a path over the cells, one feasible path in $SO(3)$ is the concatenation of geodesic paths between two neighboring sampling points or two points in one cell. Details on finding a feasible path on the cell level is given in the next section.

5 Path Planning in $SO(3)$

In this section, with the cell abstraction of $SO(3)$ and the cell-to-cell attitude sub-maneuvers, we construct a graph model to formulate the path planning problem. This section is concluded with a theoretical feasibility analysis. Recall that given R_0, R_f and the active zone \mathcal{A} , the constrained attitude path planning is to find a path $F : [0, 1] \rightarrow SO(3)$ such that $F(0) = R_0, F(1) = R_f$ and $F(t) \in \mathcal{A}$ for all $t \in [0, 1]$ or return **infeasible**.

In order to facilitate the path planning on the cell level, a graph that abstracts $SO(3)$ needs to be built. We refer to a finite vertex set V with its elements to be all the sampling cells $V := \{S_1, S_2, \dots, S_n\}$, and the edge set E to be $E := \{(S_i, S_j) \mid i \neq j, R_i \in N_j\}$.

By definition, $(S_i, S_j) \in E$ implies $(S_j, S_i) \in E$ as well. Thus, an undirected graph $\mathcal{G} = (V, E)$ is constructed as a representation of the incidence relations between the sampling cells. A *path* of length m in a graph is defined as a sequence of vertices $S_{i_0}, S_{i_1}, \dots, S_{i_m}$ such that for $k = 0, 1, \dots, m - 1$, the vertices pair $(S_{i_k}, S_{i_{k+1}}) \in E$. A single vertex is defined as a path with length 0. An induced subgraph $\mathcal{G}' = (V', E')$ is defined as $V' \subseteq V, E' := \{(S_i, S_j) \in E \mid S_i, S_j \in V'\}$. For any R_0 and $R_f \in SO(3)$, we denote by V_0 and V_f , respectively, the set of sampling cells that contain R_0 and R_f , i.e., $V_0 := \{S_i \in V \mid R_0 \in S_i\}, V_f := \{S_i \in V \mid R_f \in S_i\}$. From property (iv) of Theorem 1, $V_0 \neq \emptyset$ and $V_f \neq \emptyset$.

Based on the graph abstraction of the rotation space $SO(3)$, we show that there is an existence equivalence of a path in any induced subgraph $\mathcal{G}' = (V', E')$ and a path in the union region of cells from V' , expressed in the following Proposition.

Proposition 3 *Suppose graph $\mathcal{G}' = (V', E')$ is an induced subgraph of \mathcal{G} . A path $F(\cdot)$ exists in $\cup_i S_i$ connect-*

ing R_0 and R_f for $S_i \in V'$, if and only if a path in \mathcal{G}' exists that connects V_0 and V_f .

PROOF. *Necessity proof* Denote the index set \mathcal{N}' of V' to be $\mathcal{N}' := \{i_1, i_2, \dots, i_m\}$. Assume there exists a path $F : [0, 1] \rightarrow \cup_{i_k \in \mathcal{N}'} S_{i_k}$ connecting R_0 and R_f . A

map $M : [0, 1] \rightarrow 2^{\mathcal{N}'}$ can be defined as $M(x) := \{i_k \in \mathcal{N}' \mid F(x) \in S_{i_k}\}$ indicating the index of cells containing $F(x)$. By definition, $F(\cdot)$ is continuous. Since S_{i_k} is an open set, $\forall x_0 \in (0, 1)$, suppose $F(x_0) \in S_{i_k}$, and then there exists $\epsilon > 0$ such that $F(x) \in S_{i_k}$ for $x_0 - \epsilon < x < x_0 + \epsilon$, i.e., $\forall x \in (0, 1), \exists \epsilon > 0, M(x - \epsilon) \cap M(x + \epsilon) \neq \emptyset$. Now consider a continuous trajectory that transverse from region S_{i_j} to region $S_{i_k}, i_j, i_k \in \mathcal{N}'$. During that transverse, $M(x)$ will contain $\{i_j\}, \{i_j, i_k\}$ and $\{i_k\}$ as x increases. That implies the existence of a corresponding path from S_{i_j} to S_{i_k} in \mathcal{G}' .

Sufficiency proof Consider a path in \mathcal{G}' connecting V_0 and V_f . One possible path can be constructed as the concatenation of geodesic paths between two neighboring sampling points or between two points in one cell, as shown in Fig. 3. From Propositions 1 and 2, the designed path is guaranteed to be in $\cup_{i_k \in \mathcal{N}'} S_{i_k}$. \square

As a natural corollary, the graph \mathcal{G} has the following property. This corollary shows that based on the constructed graph abstraction \mathcal{G} , we can go from any initial attitude to any target attitude in the obstacle-free scenario.

Corollary 1 *Graph \mathcal{G} is connected.*

PROOF. For arbitrary two vertices S_l, S_k in \mathcal{G} , choose R_l, R_k , the center points of S_l, S_k , as the starting and ending point, respectively. Thus, $V_0 = \{S_l\}, V_f = \{S_k\}$. Recall that for any $R_l, R_k \in SO(3)$, R_l and R_k are connected by their geodesics. From Proposition 3, it implies that there exists a path between S_l and S_k in graph \mathcal{G} . Thus, graph \mathcal{G} is connected. \square

When there exist some obstacle regions in $SO(3)$, we need to abstract the keep-out region \mathcal{O} and the active region \mathcal{A} with sampling cells. Define the set of feasible cells by

$$V_{\mathcal{F}} := \{S_i \in V \mid \mathcal{O} \cap S_i = \emptyset\}. \quad (9)$$

Since $\mathcal{A} = SO(3) \setminus \mathcal{O}$, we deduce that for all $S_i \in V_{\mathcal{F}}, S_i \subset \mathcal{A}$. Similarly, the set of over-approximate feasible cells is defined by $V_{\overline{\mathcal{F}}} := \{S_i \in V \mid \mathcal{A} \cap S_i \neq \emptyset\}$. The feasible region \mathcal{F} and its over-approximation $\overline{\mathcal{F}}$ are defined as $\mathcal{F} := \cup_i S_i$, where $S_i \in V_{\mathcal{F}}$ and $\overline{\mathcal{F}} := \cup_i S_i$, where $S_i \in V_{\overline{\mathcal{F}}}$. Based on the definitions of $\mathcal{F}, \overline{\mathcal{F}}$, we can show that \mathcal{F} is an under-approximate region of \mathcal{A} ($\mathcal{F} \subseteq \mathcal{A}$), while $\overline{\mathcal{F}}$ is an over-approximate region of \mathcal{A} ($\mathcal{A} \subseteq \overline{\mathcal{F}}$). In fact, for any $R \in \mathcal{F}$, in view of (9), $R \notin \mathcal{O}$,

and thus $R \in \mathcal{A}$. Similarly, for any $R \in \mathcal{A}$, as the union of the sampling cells covers $SO(3)$, R must also lie in some cell $S_i \in V_{\overline{\mathcal{F}}}$, and thus $R \in \overline{\mathcal{F}}$.

Correspondingly, the induced subgraphs $\mathcal{G}_{\mathcal{F}}$ and $\mathcal{G}_{\overline{\mathcal{F}}}$ are defined as $\mathcal{G}_{\mathcal{F}} := (V_{\mathcal{F}}, E_{\mathcal{F}})$, $\mathcal{G}_{\overline{\mathcal{F}}} := (V_{\overline{\mathcal{F}}}, E_{\overline{\mathcal{F}}})$, where $E_{\mathcal{F}} = \{(S_i, S_j) \in E \mid S_i, S_j \in V_{\mathcal{F}}\}$, $E_{\overline{\mathcal{F}}} = \{(S_i, S_j) \in E \mid S_i, S_j \in V_{\overline{\mathcal{F}}}\}$. The algorithm for the graph abstraction is summarized in Algorithm 2.

Algorithm 2 Graph abstraction for the active region \mathcal{A} .

Input: $\mathcal{O}, \mathcal{A}, R_0, R_f, U, \theta$, sampling set U, θ
Output: $\mathcal{G}_{\mathcal{F}}$ and $\mathcal{G}_{\overline{\mathcal{F}}}$

initialization :

- 1: from R_0, R_f, U, θ , construct \mathcal{G}, V_0, V_f
- 2: define $V_{\mathcal{F}} = V, V_{\overline{\mathcal{F}}} = \{ \}$
- construct the subgraphs:*
- 3: **for** each R_o in \mathcal{O} **do**
- 4: **for** R_i in U **do**
- 5: **if** $d(R_o, R_i) \leq \theta$ and $S_i \in V_{\mathcal{F}}$ **then**
- 6: $V_{\mathcal{F}} \leftarrow V_{\mathcal{F}}$ with the node S_i removed
- 7: **end if**
- 8: **end for**
- 9: **end for**
- 10: construct $\mathcal{G}_{\mathcal{F}}$ from $V_{\mathcal{F}}$ and \mathcal{G}
- 11: **for** each R_a in \mathcal{A} **do**
- 12: **for** R_i in U **do**
- 13: **if** $d(R_a, R_i) < \theta$ and $S_i \notin V_{\overline{\mathcal{F}}}$ **then**
- 14: $V_{\overline{\mathcal{F}}} \leftarrow V_{\overline{\mathcal{F}}}$ with the node S_i added
- 15: **end if**
- 16: **end for**
- 17: **end for**
- 18: construct $\mathcal{G}_{\overline{\mathcal{F}}}$ from $V_{\overline{\mathcal{F}}}$ and \mathcal{G}

Remark 2 In Algorithm 2, the regions \mathcal{O} and \mathcal{A} usually contain infinite elements. When implementing Algorithm 2, we first generate a large number of random rotations. Those rotations that lie in \mathcal{O} are then used to construct $\mathcal{G}_{\mathcal{F}}$ in step 3; otherwise, they are used to construct $\mathcal{G}_{\overline{\mathcal{F}}}$ in step 11.

With a finite graph model abstracting the active regions \mathcal{A} , the process of finding a feasible path is tractable by many classic complete graph search algorithms, such as Dijkstra’s algorithm or A^* algorithm [19]. These search algorithms are guaranteed to find a path in a finite graph if it exists or terminate otherwise.

Assume that a path $S_{i_0}S_{i_1} \dots S_{i_m}$ of length m in $\mathcal{G}_{\mathcal{F}}$ is found that connects V_0 and V_f . The feasible path in $\mathcal{G}_{\mathcal{F}}$ is thus the concatenation of geodesic paths between $R_0R_{i_0}R_{i_1} \dots R_{i_m}R_f$, where R_{i_k} is the sampling point of cell S_{i_k} for $k = 0, 1, \dots, m$. Propositions 1 and 2 guarantee that this path lies in \mathcal{F} , and thus in \mathcal{A} . An illustration on how the attitude transfers from R_0 to R_f is shown in Fig. 3.

To establish how complete our algorithm is in terms of finding a path in \mathcal{A} , we provide a sufficient condition and a necessary condition separately for arbitrary constrained zones.

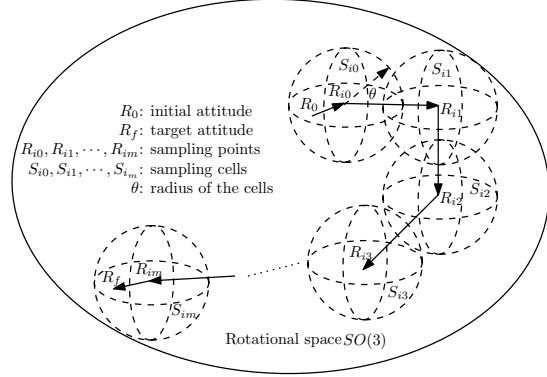


Fig. 3. An illustration of cell-to-cell attitude maneuvering.

Corollary 2 (Sufficient condition) *If there exists a path in $\mathcal{G}_{\mathcal{F}}$ connecting V_0 and V_f , then there exists a path in \mathcal{A} connecting R_0 and R_f .*

PROOF. Recall $\mathcal{F} \subseteq \mathcal{A}$. From Proposition 3, if there exists a feasible solution in \mathcal{F} , then there exists one path in graph $\mathcal{G}_{\mathcal{F}}$, and vice versa. Thus, a path in $\mathcal{G}_{\mathcal{F}}$ connecting V_0 and V_f indicates that a path exists in \mathcal{F} connecting R_0 and R_f , which further implies that a path exists in \mathcal{A} connecting R_0 and R_f . \square

Corollary 3 (Necessary condition) *If there exists a path in \mathcal{A} connecting R_0 and R_f , then there exists a path in $\mathcal{G}_{\overline{\mathcal{F}}}$ connecting V_0 and V_f .*

PROOF. Similarly, recall $\mathcal{A} \subseteq \overline{\mathcal{F}}$. From Proposition 3, if there exists a feasible solution in $\overline{\mathcal{F}}$, then there exists one path in graph $\mathcal{G}_{\overline{\mathcal{F}}}$, and vice versa. A path in \mathcal{A} connecting R_0 and R_f indicates that a path in $\overline{\mathcal{F}}$ connecting R_0 and R_f , and thus implies a path in $\mathcal{G}_{\overline{\mathcal{F}}}$ connecting V_0 and V_f . \square

Based on these two corollaries, we can reason about the existence of a path in \mathcal{A} based on the graph search results on $\mathcal{G}_{\mathcal{F}}$ and $\mathcal{G}_{\overline{\mathcal{F}}}$ at a fixed sampling step s . The search algorithm gives out three possible feasibility results, categorized as **feasible problem** (a path in $\mathcal{G}_{\mathcal{F}}$ is found), **infeasible problem** (no path in $\mathcal{G}_{\overline{\mathcal{F}}}$ is found), or **infeasible problem at the present s** (no path in $\mathcal{G}_{\mathcal{F}}$ is found but a path in $\mathcal{G}_{\overline{\mathcal{F}}}$ is found). For the first case, the search algorithm will generate a path in \mathcal{F} , thus in \mathcal{A} . Moreover, when $s \rightarrow 0$, the feasible region \mathcal{F} approximates \mathcal{A} in the sense of Haar Measure, i.e., the measure of $\mathcal{A} - \mathcal{F}$ approaches to 0 as $s \rightarrow 0$.

Remark 3 *Note that since the graph is finite and constructed at a given sampling step (resolution level), the completeness of the search algorithm can be seen as a resolution completeness. Therefore, it is guaranteed that we will find a feasible path in finite time when one exists at that resolution.*

6 Control Law Design

In this section, assume that we have obtained (as an output of the planning module) a feasible path consisting of the sequence $R_0 R_{i_0} R_{i_1} \dots R_{i_m} R_f$ where R_{i_1}, \dots, R_{i_m} are m intermediate sampling points corresponding to the cells S_{i_1}, \dots, S_{i_m} that lie within the active space \mathcal{A} , see Figure 3. Our objective is to generate a reference attitude trajectory $R_r(t)$ that passes through these points along geodesics and then develop a feedback control law u to track the obtained reference attitude trajectory. For convenience of notation, we re-denote the feasible path as $R_{r_0} R_{r_1} R_{r_2} \dots R_{r_L}$, where $L = m + 2$, and define the index set $\mathcal{N}_r := \{0, 1, 2, \dots, L\}$.

6.1 Reference Attitude Trajectory

In what follows, a smooth reference trajectory is derived which satisfies the attitude reference dynamics and passes through the designed feasible path. The reference trajectory between any two points of the feasible path is generated along the geodesic so that the obtained overall trajectory remains in the active region \mathcal{A} as shown in Propositions 1 and 2.

Recall that the total desired maneuvering time is T_f . Now consider a rest-to-rest reference attitude maneuver between R_{r_i} and $R_{r_{i+1}}$ for $i \in \mathcal{N}_r \setminus \{L\}$. For simplicity, we assume that the maneuvering times between any two points R_{r_i} and $R_{r_{i+1}}$ are identical and defined by $T = T_f/L$. Denote the intermediate maneuver time instants as $t_i = iT$, $i \in \mathcal{N}_r$, such that our desired reference trajectory satisfies $R_r(t_i) = R_{r_i}$. The dynamics of the reference attitude system are given by

$$\begin{cases} \dot{R}_r = R_r [\omega_r]_{\times}, \\ J\dot{\omega}_r + [\omega_r]_{\times} J\omega_r = u_r, \end{cases} \quad (10)$$

where $R_r \in SO(3)$ represents the reference attitude, $\omega_r \in \mathbb{R}^3$ is the reference angular velocity, and $u_r \in \mathbb{R}^3$ is the reference control input.

We consider the following formulation of the attitude reference trajectory that maneuvers along the geodesic between two waypoints of the path,

$$R_r(t) = \begin{cases} R_{r_i} \exp(\tau(t) A_i) & \text{for } t \in [t_i, t_{i+1}), i \in \mathcal{N}_r \setminus \{L\}, \\ R_f & \text{for } t \geq T_f. \end{cases} \quad (11)$$

where $A_i := \log(R_{r_i}^\top R_{r_{i+1}})$ and $\tau : \mathbb{R}_{\geq} \rightarrow [0, 1]$ is a scalar-valued function to be defined. In particular, we consider a piecewise continuous function $\tau(\cdot)$ (inspired from [15]) as given below, for $i \in \mathcal{N}_r \setminus \{L\}$,

$$\tau(t) = \begin{cases} \frac{t - t_i}{T} - \frac{1}{2\pi} \sin\left(\frac{2\pi(t - t_i)}{T}\right), & t \in [t_i, t_{i+1}), \\ 1, & t \geq T_f. \end{cases} \quad (12)$$

One can show that $\tau(t) = 0$ for $t = t_i, i \in \mathcal{N}_r \setminus \{L\}$ and $\dot{\tau}(t)$ is not defined for $t = t_i, i \in \mathcal{N}_r$. Defining $\dot{\tau}(t) := 0$ at those time instants, one can further show that $\dot{\tau}(t), \ddot{\tau}(t)$ not only exist but also are continuous and bounded. These properties are useful as we could obtain: 1) a differentiable reference attitude in (11) that satisfies the end-point requirement; 2) a continuous and bounded control torque. Here we note that this function is just one example and many other functions may be found that satisfy similar properties.

Then, invoking the reference attitude dynamics in (10), the reference angular velocity $\omega_r(t)$ is obtained $\omega_r(t) = \dot{\tau}(t) \exp(-\tau(t) A_i) A_i^\vee$, which is a differentiable function of t . Taking the derivative of $\omega_r(t)$, we have $\dot{\omega}_r(t) = \ddot{\tau}(t) \exp(-\tau(t) A_i) A_i^\vee - \dot{\tau}^2(t) A_i \exp(-\tau(t) A_i) A_i^\vee$. Finally, the reference control law is derived from (10) as

$$u_r = J\dot{\omega}_r + [\omega_r]_{\times} J\omega_r \quad (13)$$

with $\omega_r(t), \dot{\omega}_r(t)$ defined above.

Theorem 2 Consider the attitude dynamics in (1), the obstacle region \mathcal{O} , and the initial and the target attitudes R_0, R_f . Suppose that the planning module generates a feasible path as $R_{r_0} R_{r_1} R_{r_2} \dots R_{r_L}$ and the attitude maneuver starts from R_0 , $\omega(0) = 0$. With the control $u = u_r$ in (13) applied, the attitude will follow exactly the reference motion described in (11) and reach R_f at the time instant T_f while avoiding the obstacle region \mathcal{O} , i.e., $R(t) = R_r(t) \in SO(3) \setminus \mathcal{O}$ for $0 \leq t \leq T_f$, $R(T_f) = R_f$.

PROOF. The attitude reference is constructed based on the concatenation of geodesic paths between $R_{r_0} R_{r_1} R_{r_2} \dots R_{r_L}$. Note $R_{r_0} = R_0, R_{r_L} = R_f, R_{r_i} \in V_{\mathcal{F}}$ for $i \in \mathcal{N}_r \setminus \{0, L\}$. Propositions 1 and 2 state that the sub-maneuver between $(R_{r_i}, R_{r_{i+1}}), i \in \mathcal{N}_r \setminus \{L\}$ along the geodesic lies within the feasible region $\mathcal{F} \subset SO(3) \setminus \mathcal{O}$. As the control signal is based on the inverse of the differentiating process, which is omitted here, the actual attitude will follow exactly the reference motion and thus reach R_f at the time instant T_f while avoiding the obstacle region \mathcal{O} . \square

6.2 Attitude Error Dynamics and Controller Design

In the presence of perturbations the feed-forward controller alone is not sufficient to stabilize the attitude trajectory around the reference trajectory. Hence we derive an attitude feedback control law to track the reference trajectory generated above. Let us define the attitude error $\tilde{R}(t) := R_r^\top R$, and the angular velocity error² $\tilde{\omega}(t) := \omega - \tilde{R}^\top \omega_r$ where R_r and ω_r are the reference

² This angular velocity error has been widely used in the field of attitude control and represents the error between the body-frame angular velocity ω and the body-frame representation, namely $\tilde{R}\omega_r$, of the reference angular velocity ω_r such that both quantities are compared in the same frame.

attitude and angular velocity specified in the previous subsection. In view of (1) and (10), we derive the attitude error dynamics

$$\begin{cases} \dot{\tilde{R}} = \tilde{R}[\tilde{\omega}]_{\times}, \\ J\dot{\tilde{\omega}} = f(\tilde{R}, \tilde{\omega}, \omega_r)\tilde{\omega} - J\tilde{R}^{\top}\dot{\omega}_r - [\tilde{R}^{\top}\omega_r]_{\times}J\tilde{R}^{\top}\omega_r + u, \end{cases} \quad (14)$$

where $f(\tilde{R}, \tilde{\omega}, \omega_r) = [J\tilde{\omega}]_{\times} + [J\tilde{R}^{\top}\omega_r]_{\times} - [\tilde{R}^{\top}\omega_r]_{\times}J - J[\tilde{R}^{\top}\omega_r]_{\times}$ is a skew-symmetric matrix. We then propose the following attitude control law

$$u := J\tilde{R}^{\top}\dot{\omega}_r + [\tilde{R}^{\top}\omega_r]_{\times}J\tilde{R}^{\top}\omega_r - k_1(\tilde{R} - \tilde{R}^{\top})^{\vee} - k_2 \tanh(\tilde{\omega}), \quad (15)$$

where $k_1, k_2 > 0$ are tuning gains and $\tanh(\cdot)$ is the element-wise hyperbolic tangent function.

Proposition 4 Consider the attitude error dynamics in (14) with the reference motion described in (11). Under the feedback law (15), the equilibrium $(\tilde{R}, \tilde{\omega}) = (I, 0)$ is asymptotically stable.

The control law consists of the feedforward term (first two terms) that coincides with the reference control law when there exists no attitude error ($\tilde{R} = I$) and the feedback term (the last two terms) that robustly tracks the reference attitude. This controller shares a similar structure with other recent attitude tracking works such as [20] except that we use here the saturation function $\tanh(\cdot)$ to bound the control *a priori*. The proof for Proposition 4 can be derived following similar steps as in [20] and thus omitted here.

Furthermore, the control signal u in (15) is bounded by $\|u\|_2 \leq \lambda_{\max}(J)\|\dot{\omega}_r\|_2 + \lambda_{\max}(J)\|\omega_r\|_2^2 + 2k_1 + \sqrt{3}k_2$, where we used $\|(\tilde{R} - \tilde{R}^{\top})^{\vee}\|_2 = \|\tilde{R} - \tilde{R}^{\top}\|_F/\sqrt{2} \leq 2$, $\|\tanh(\tilde{\omega})\|_2 \leq \sqrt{3}$. From the reference trajectory in (11) and $\tau(t)$ in (12), we further have $\|\omega_r\|_2 \leq 4\theta/T$, $\|\dot{\omega}_r\|_2 \leq (4\pi\theta + 16\theta^2)/T^2$, where θ is the radius of the sampling cells. Thus, it follows $\|u\|_2 < \lambda_{\max}(J)(4\pi\theta + 32\theta^2)/T^2 + 2k_1 + \sqrt{3}k_2$. Based on this explicit bound, one can choose T, k_1, k_2 such that $T > \sqrt{\lambda_{\max}(J)(4\pi\theta + 32\theta^2)/u_{\max}}$, $0 < k_1 \leq (u_{\max} - \Delta)/4$, $0 < k_2 \leq (u_{\max} - \Delta)/2\sqrt{3}$, where $\Delta := \lambda_{\max}(J)(4\pi\theta + 32\theta^2)/T^2$. Thus the control input constraints are imposed.

7 Simulations

In this section, we will show a numerical simulation of our proposed method for non-convex obstacles. The inertia matrix of the rigid body is given by $J = \begin{bmatrix} 5.5 & 0.06 & -0.03 \\ 0.06 & 5.5 & 0.01 \\ -0.03 & 0.01 & 0.1 \end{bmatrix} \text{kg} \cdot \text{m}^2$. Setting the initial sampling step $s = 2\sin(\pi/24)$, then the corresponding cell sampling has 4392 sampling points with a radius $\theta = 0.2269$ rad (13°). u_{\max} is set to be

$2 \text{ N} \cdot \text{m}$. The simulation result is conducted with a perturbed attitude model under additive disturbance $d(t) = 0.25 \times \begin{bmatrix} 0.15 \sin(0.5t) + 0.05 \\ 0.15 \cos(0.5t) - 0.05 \\ 0.1 \sin(0.5t) + 0.01 \cos(0.5t) \end{bmatrix} \text{N} \cdot \text{m}$ on the actuator.

Suppose the constrained zones $\mathcal{O} := \mathcal{O}_A \setminus \mathcal{M}$, where $\mathcal{O}_A := \cup_i \{R \mid \langle \mathbf{a}_i, R\mathbf{a}_0 \rangle \geq \cos \alpha_i\}$, $i = 1, 2, 3, 4$, $\mathcal{M} := \{R \in SO(3) \mid \langle \mathbf{b}, R\mathbf{a}_0 \rangle \geq \cos \gamma\}$, $\mathbf{a}_0 = (1, 0, 0)^{\top}$, $\mathbf{a}_1 = (0.174, -0.934, -0.034)^{\top}$, $\mathbf{a}_2 = (0, 0.7071, 0.7071)^{\top}$, $\mathbf{a}_3 = (-0.853, 0.436, -0.286)^{\top}$, $\mathbf{a}_4 = (-0.122, -0.140, -0.983)^{\top}$, $\mathbf{b} = (0.5080, -0.8606, -0.0358)^{\top}$, $\alpha_1 = \alpha_2 = \alpha_3 = 40^\circ$, $\alpha_4 = 20^\circ$, $\gamma = 25^\circ$. The obstacle zone is thus non-convex. The initial attitude is set as $R(0) = \exp(135^\circ/180^\circ \times \pi[e_3]_{\times})$ with an initial angular velocity of $\omega(0) = 0$ rad/s. The target attitude is $R_f = \begin{bmatrix} 0.3472 & 0 & -0.9378 \\ -0.9149 & -0.2195 & -0.3387 \\ -0.2058 & 0.9756 & -0.0762 \end{bmatrix}$.

With the initial sampling step $s = 2\sin(\pi/24)$, the planning algorithm gives out **infeasible at the present resolution**. Then we refine the sampling step to $s = 2\sin(\pi/36)$ and $\theta = 0.1396$ rad (8 degrees). At this resolution, the planning algorithm gives us a feasible path with 16 steps. The planned trajectory and the actual trajectory are depicted in Fig. 4. For a better illustration, Fig. 4(a) and Fig. 4(b) are obtained from two different viewpoints, where the initial attitude and the target attitude are denoted as the diamond and the cross, respectively. More details on the attitude maneuver and tracking errors are shown in Fig. 5. One can see that after T_f (80s), the tracking error is always less than 2° . Also, as shown in Fig. 5(b), the control input remains bounded by u_{\max} for all times.

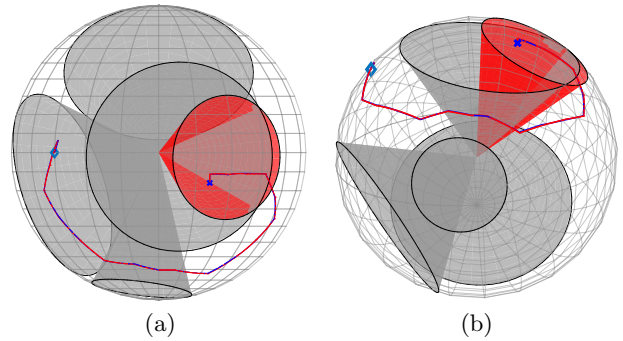


Fig. 4. Attitude maneuvering trajectory (two viewpoints).

We also observe in simulation that given \mathcal{O}, R_0, R_f , a finer sampling can yield a feasible path while a coarse sampling may not. However, a smaller sampling step will generate more transitions and lead to a growing computational time during planning and a larger control input limit (assuming that T_f is fixed).

8 Conclusion

In this paper, we developed a new framework for the constrained attitude maneuver problem. The framework

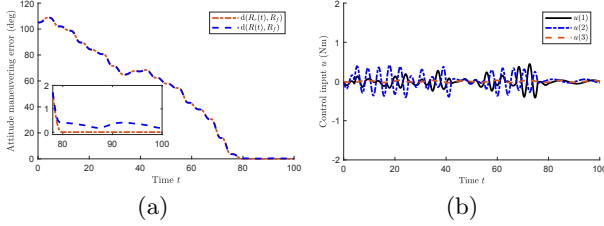


Fig. 5. The attitude maneuvering error (a) and the control signal $u(t)$ (b) versus time.

consists of three main components: rotation space sampling, planning and low-level control. For each component, the corresponding theoretical guarantees are given. First, the sampling cells are constructed as overlapping cells in $SO(3)$ with an identical radius around the sampling points. The obtained sampling cells have the nice properties that their union covers the whole rotation space $SO(3)$ and are distributed such that every sampling point (center of the cell) is contained in one single cell. Then, the proposed planning algorithm is resolution complete for a given sampling step and it terminates when the original problem is infeasible. The sampling and planning computations are all performed offline. Once a feasible path in the abstracted graph is obtained, the smooth reference trajectory is generated by following the geodesic on $SO(3)$. Next, a feedback control law is designed to ensure that the true attitude trajectory will follow the reference trajectory in presence of perturbations. The proposed strategy can handle a general class of constrained zones with a pre-defined control input bound. Numerical simulation is performed in the case of non-convex obstacle regions and validates the desirable features of this constrained control approach on $SO(3)$.

References

- [1] Daniel E Koditschek. Application of a new lyapunov function to global adaptive attitude tracking. In *Proceedings of the 27th IEEE Conference on Decision and Control*, pages 63–68, 1988.
- [2] Amit Sanyal, Adam Fosbury, Nalin Chaturvedi, and Dennis Bernstein. Inertia-free spacecraft attitude tracking with disturbance rejection and almost global stabilization. *Journal of Guidance, Control, and Dynamics*, 32(4):1167–1178, 2009.
- [3] Ramaprakash Bayadi and Ravi N Banavar. Almost global attitude stabilization of a rigid body for both internal and external actuation schemes. *European Journal of Control*, 20(1):45–54, 2014.
- [4] Soulaïmane Berkane, Abdelkader Abdessameud, and Abdelhamid Tayebi. Hybrid global exponential stabilization on $SO(3)$. *Automatica*, 81:279–285, 2017.
- [5] Hari B Hablani. Attitude commands avoiding bright objects and maintaining communication with ground station. *Journal of Guidance, Control, and Dynamics*, 22(6):759–767, 1999.
- [6] Unsik Lee and Mehran Mesbahi. Feedback control for spacecraft reorientation under attitude constraints via convex potentials. *IEEE Transactions on Aerospace and Electronic Systems*, 50(4):2578–2592, 2014.
- [7] Shankar Kulamani and Taeyoung Lee. Constrained geometric attitude control on $SO(3)$. *International Journal of Control, Automation and Systems*, 15(6):2796–2809, 2017.
- [8] Qiang Shen, Chengfei Yue, Cher Hiang Goh, Baolin Wu, and Danwei Wang. Rigid-body attitude stabilization with attitude and angular rate constraints. *Automatica*, 90:157–163, 2018.
- [9] E Frazzoli, MA Dahleh, E Feron, and R Kornfeld. A randomized attitude slew planning algorithm for autonomous spacecraft. In *AIAA Guidance, Navigation, and Control Conference*, 2001.
- [10] Henri C Kjellberg and E Glenn Lightsey. Discretized quaternion constrained attitude pathfinding. *Journal of Guidance, Control, and Dynamics*, 38(11):713–718, 2015.
- [11] Qinglei Hu, Biru Chi, and Maruthi R Akella. Anti-unwinding attitude control of spacecraft with forbidden pointing constraints. *Journal of Guidance, Control, and Dynamics*, pages 1–13, 2018.
- [12] Julie C Mitchell. Sampling rotation groups by successive orthogonal images. *SIAM Journal on Scientific Computing*, 30(1):525–547, 2008.
- [13] D Roşca, A Morawiec, and M De Graef. A new method of constructing a grid in the space of 3d rotations and its applications to texture analysis. *Modelling and Simulation in Materials Science and Engineering*, 22(7):075013, 2014.
- [14] Anna Yershova, Swati Jain, Steven M Lavalle, and Julie C Mitchell. Generating uniform incremental grids on $SO(3)$ using the Hopf fibration. *The International Journal of Robotics Research*, 29(7):801–812, 2010.
- [15] James D Biggs and Lucy Colley. Geometric attitude motion planning for spacecraft with pointing and actuator constraints. *Journal of Guidance, Control, and Dynamics*, 39(7):1672–1677, 2016.
- [16] Francesco Bullo and Andrew D Lewis. *Geometric control of mechanical systems: modeling, analysis, and design for simple mechanical control systems*, volume 49. Springer Science & Business Media, 2004.
- [17] Malcolm D Shuster. A survey of attitude representations. *Journal of the Astronautical Sciences*, 41(4):439–517, 1993.
- [18] Ken Shoemake. Animating rotation with quaternion curves. In *ACM SIGGRAPH Computer Graphics*, volume 19, pages 245–254. ACM, 1985.
- [19] Thomas H Cormen, Charles E Leiserson, Ronald L Rivest, and Clifford Stein. *Introduction to algorithms*. MIT press, 2009.
- [20] Taeyoung Lee. Robust adaptive attitude tracking on $SO(3)$ with an application to a quadrotor uav. *IEEE Transactions on Control Systems Technology*, 21(5):1924–1930, 2012.